Comparison Study for Whitney (Raviart-Thomas) Type Source Models in Finite Element Method Based EEG Forward Modeling

Martin Bauer, Sampsa Pursiainen, Johannes Vorwerk, Harald Köstler, Carsten H.Wolters

***Abstract*—This study concentrates on finite element method (FEM) based electroencephalography (EEG) forward simulation in which the electric potential evoked by neural activity in the brain is to be calculated at the surface of the head. The main advantage of the FEM is that it allows realistic modeling of tissue conductivity inhomogeneity. However, it is not straightforward to apply the classical model of a dipolar source with the FEM, due to its strong singularity and the resulting irregularity. The focus of this study is on comparing different methods to cope with this problem. In particular, we evaluate the accuracy of Whitney (Raviart-Thomas) type dipole-like source currents compared to two reference dipole modeling methods: the St. Venant and partial integration approach. Common to all these methods is that they enable direct approximation of the potential field utilizing linear basis functions. In the present context, Whitney elements are particularly interesting, as they provide a simple means to model a divergence-conforming primary current vector field satisfying the square integrability condition. Our results show that a Whitney type source model can provide simulation accuracy comparable to the present reference methods. It can lead to superior accuracy under optimized conditions with respect to both source location and orientation in a tetrahedral mesh. For random source orientations, the St. Venant approach turns out to be the method of choice over the interpolated version of the Whitney model. The overall moderate differences obtained suggest that practical aspects, such as the focality, should be prioritized when choosing a source model.**

I. Introduction

This study concentrates on finite element method (FEM) based electroencephalography (EEG) forward simulation in which the electric potential field evoked by neural activity is to be approximated given the geometry, conductivity distribution and a primary source current field of the target domain [1], [2], [3], [4], [5]. With respect to the current standard in EEG forward simulation, that is, the boundary element method (BEM) coupled with a compartment-wise isotropic and homogeneous volume conductor model [5], [6], [7], [8], [9], 3D approaches such as the FEM or the finite difference method (FDM) constitute a substantial improvement, as they enable modeling of the strongly folded outer brain surface [10], [11], detailed structures of skull compacta and spongiosa [12], [11], and the distinctly anisotropic conductivity of the white matter [13], [14], [11]. Today, the use of fully realistic 3D conductivities is accessible even with a standard laptop or desktop computer, making the FEM attractive regarding any computational application of EEG. A crucial point in FEM forward simulation is the source current distribution. Namely, the classical dipole source cannot be directly applied, since the forward problem in its weak form necessitates the divergence of the source to be square integrable [15].

Manuscript received March 1, 2015. Accepted for publication May 19, 2015.

M. Bauer and H. Köstler are with the Department of Computer Science 10, Friedrich-Alexander-University Erlangen-Nürnberg, Germany.

S. Pursiainen (corresponding author) is with the Department of Mathematics and Systems Analysis, Aalto University, Helsinki, Finland and the Department of Mathematics, Tampere University of Technology, Finland.

C. Wolters and J. Vorwerk are with Institute for Biomagnetism and Biosignalanalysis, University of Münster, Germany.

Several approaches to approximate a dipolar source in the brain and calculate the resulting potential distribution have been developed [16], [17], including the reference methods used here: the St. Venant [18], [19], [20] and partial integration (PI) approaches [21], [22]. The St. Venant method approximates a dipole source via placing monopolar loads on all nodes neighboring the source position, and in PI, the right-hand side of the potential field equation is integrated by parts resulting in a non-singular and solvable form despite the presence of dipoles. Common to both methods is that they enable direct approximation of the potential field via linear finite element basis functions.

Our study focuses on the accuracy of Whitney (Raviart-Thomas) type finite elements as dipole-like source currents introduced and previously studied in [23], [24], [25]. Whitney basis functions span a piecewise linear and divergence-conforming vector field. They are the simplest ones that are mathematically directly compatible with the potential equation, meaning that their divergence is square integrable. One can use them to simulate both highly localized dipole-like currents and globally supported vector fields, which is beneficial regarding realistically modeling current distributions with finite support. Being composed of first order polynomials they are also easily accessible from the implementation point of view.

The objective of this study is a detailed evaluation of the numerical accuracy of the Whitney source model and, in particular, to find out how it performs in comparison to the St. Venant and PI approaches. Our study includes analysis for both optimized sources with regard to location and orientation and arbitrary ones to enable unbiased comparison to the reference models. Performance of a source model is investigated both within a single element as well as in a global scope via relative difference and magnitude measure (RDM and MAG) between a numerical and analytical solution within a four-layer spherical test domain. The results are evaluated using a statistical approach [26] in which accuracy and robustness of dipole approximation is analyzed via box-plots covering a wide range for the source eccentricity, i.e., relative norm of the dipole position within the brain compartment.

This paper has been organized as follows. Section II describes the tested source models as well as our experimental setup. Section III reports the outcome of the numerical experiments followed by the discussion in Section IV. Finally, the appendix includes some essential theoretical background regarding the Whitney source model.

II. Materials and Methods

A. Forward Model

The goal of the EEG forward problem is to predict the (quasi-static) electric potential field u on the surface $\partial\Omega$ of the domain Ω, given the symmetric and positive definite distribution of conductivity tensors σ and the primary current field $\vec{J}^P$ in Ω. This corresponds to solving the Poisson type equation $\nabla\cdot(\sigma\nabla u) = \nabla\cdot\vec{J}^P$ in Ω equipped with the homogeneous Neumann boundary condition $(\sigma\nabla u)\cdot\vec{n} = 0$ on $\partial\Omega$. This equation multiplied by a test function v and integrated

by parts yields the weak form

$$\int_\Omega \nabla v \cdot (\sigma \nabla u)\, dV = -\int_\Omega v(\nabla \cdot \vec{J}^P)\, dV \quad \text{for all } v \in H^1(\Omega) \quad (1)$$

in which $H^1(\Omega)$ denotes the Sobolev space consisting of functions with all first-order partial derivatives square integrable, i.e., in $L_2(\Omega)$. The weak form has a solution $u \in H^1(\Omega)$ that is unique up to choosing the zero level of the potential if $\nabla \cdot \vec{J}^P \in L_2(\Omega)$ [15], [27], [3].

Whitney (Raviart-Thomas) basis functions are the simplest piecewise first-order polynomials that have this property due to continuous vector field normal component over the element faces [28], [29], [3]. Consequently, they provide a mathematically rigorous framework for modeling finitely supported source currents. The reference source models of this paper do not rely on vector-valued basis functions. Instead, they approximate the dipolar source by a distribution of electrical monopoles placed on finite element nodes in its vicinity. Note that an actual dipole source does not have a square integrable divergence, meaning that it needs to be modeled asymptotically in a numerical simulation.

In this paper, the potential distribution is approximated via the sum $u_h = \sum_{i=1}^N z_i \psi_i$ in which $\psi_1, \psi_2, \ldots, \psi_N$ are linear nodal basis functions belonging to $H^1(\Omega)$. The coefficient vector $\mathbf{z} = (z_1, z_2, \ldots, z_N)$ refers to the solution of the linear system $\mathbf{Az} = \mathbf{f}$ with $A_{i,j} = \int_\Omega \nabla\psi_j \cdot (\sigma \nabla \psi_i)\, dV$ and with $\mathbf{f}$ denoting a model-specific right-hand side vector.

B. Whitney Type Source Model

If the primary current field is a linear sum $\vec{J}^P = \sum_{k=1}^M x_k \vec{w}_k$ of Whitney basis functions $\vec{w}_1, \vec{w}_2, \ldots, \vec{w}_M$, the entries of $\mathbf{f}$ are of the form

$$f_i = -\sum_{k=1}^M x_k \int_\Omega \psi_i (\nabla \cdot \vec{w}_k)\, dV. \quad (2)$$

Following from (2), one can write $\mathbf{f} = \mathbf{Gx}$, where $\mathbf{x} = (x_1, x_2, \ldots, x_M)$ and $\mathbf{G}$ is a basis transfer matrix given by $G_{i,k} = -\int_\Omega (\nabla \cdot \vec{w}_k)\, \psi_i\, dV$. Based on the solution u_h, electrode voltages on the surface $\partial\Omega$ can be obtained by restricting u_h to those cofficients that correspond to the targeted points (electrodes), i.e., evaluating $\mathbf{Tf} = \mathbf{RA}^{-1}\mathbf{f}$, where $\mathbf{R}$ is a restriction matrix. Essential in this procedure is the so-called transfer matrix $\mathbf{T} = \mathbf{RA}^{-1}$ which can be computed by solving a set of linear systems, one for each electrode [30].

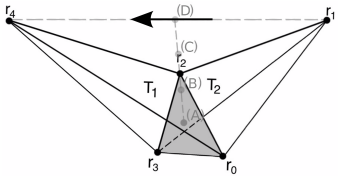

Fig. 1. Whitney Basis Function supported on two tetrahedra T_1 and T_2 with source locations (A)–(D) and resulting synthetic dipole for (D) shown by the arrow.

1) Whitney Basis Functions for a Tetrahedral Mesh: In a tetrahedral mesh, the face-based Whitney basis function $\vec{w}$ is supported in two adjacent tetrahedra T_1 and T_2 (Figure 1) sharing the face F. As indicated in the appendix, one can write

$$\vec{w}(\vec{r}) = \begin{cases} \dfrac{\vec{r}_4 - \vec{r}}{3\, V_{T_1} \|\vec{r}_4 - \vec{r}_1\|}, & \text{if} \quad \vec{r} \in T_1 \\ \dfrac{\vec{r} - \vec{r}_1}{3\, V_{T_2} \|\vec{r}_4 - \vec{r}_1\|}, & \text{if} \quad \vec{r} \in T_2 \\ 0, & \text{otherwise} \end{cases} \quad (3)$$

in which $\vec{r}_1$ and $\vec{r}_4$ are the positions of vertices 1 and 4 in Figure 1 and V_{T_1} and V_{T_2} are the volumes of T_1 and T_2, respectively. That is, the restriction of $\vec{w}$ to a single element is a first order polynomial, equivalent to the position vector field transferred and scaled. The total vector field is zero at vertices 1 and 4 opposite to the face F. Its normal component is continuous on F and vanishes on all other faces [28], [29], [3].

A basis function $\vec{w}$ is given a synthetic dipole moment

$$\vec{q}_{\vec{w}} = \int_\Omega \vec{w}\, dV = \frac{\vec{r}_4 - \vec{r}_1}{\|\vec{r}_4 - \vec{r}_1\|} \quad \text{with} \quad \|\vec{q}\| = 1 \quad (4)$$

and position $\vec{r}_w = \sum_{i=0}^4 \alpha_i \vec{r}_i$, i.e., a linear combination of vertices $\vec{r}_0, \vec{r}_1, \ldots, \vec{r}_4$ (Figure 1). Four different combinations (A)–(D) for the coefficients $\alpha_0, \alpha_1, \ldots, \alpha_4$ suggested in [24] and listed in Table I are studied. In Figure 1, the points corresponding to (A)–(D) lie in a respective order on a single line between the center (A) of the face F and the midpoint (D) of the line segment between $\vec{r}_1$ and $\vec{r}_4$, i.e.,

$$\vec{r}_{\vec{w}}^{\,(D)} = \frac{1}{2}(\vec{r}_1 + \vec{r}_4). \quad (5)$$

Consequently, point (A) is located where the norm of the vector field basis function $\vec{w}$ is large, whereas (D) approximates the focus of the divergence distribution $\nabla \cdot \vec{w}$ that is supported by the nodal basis functions associated with the nodes $\vec{r}_1$ and $\vec{r}_4$ (see [24]). In applications, relevance of these points can vary whether the source current distribution is handled directly as a vector field or indirectly via its divergence.

Location	α_0	α_1	α_2	α_3	α_4
A	1/3	0	1/3	1/3	0
B	1/5	1/5	1/5	1/5	1/5
C	1/9	1/3	1/9	1/9	1/3
D	0	1/2	0	0	1/2

TABLE I
CANDIDATES FOR SOURCE LOCATION [24].

A position based optimization (PBO) strategy developed for this study is applied for interpolation of the Whitney sources [31]. A given dipole with moment (a coordinate vector) $\mathbf{p} = (p_1, p_2, p_3)$ and location $\vec{r}$ was approximated via the synthetic parameters $\mathbf{q}_{\vec{w}_\ell}$ (coordinate vector form) and $\vec{r}_{\vec{w}_\ell}$, $\ell = 1, 2, 3, 4$ that can be associated with the four faces of the tetrahedron containing $\vec{r}$. In order to minimize piling of errors, the task was to find a solution for the optimization problem

$$\min_{\mathbf{c}} \sum_{\ell=1}^4 c_\ell^2 \omega_\ell^2 \quad \text{subject to} \quad \mathbf{Qc} = \mathbf{p}, \quad (6)$$

where $\mathbf{c} = (c_1, c_2, c_3, c_4)$ and $\omega_\ell = \|\vec{r}_{\vec{w}_\ell} - \vec{r}\|_2$ is a weighting coefficient and $\mathbf{Q} = (\mathbf{q}_{\vec{w}_1}, \mathbf{q}_{\vec{w}_2}, \mathbf{q}_{\vec{w}_3}, \mathbf{q}_{\vec{w}_4})$. For the convexity of $\sum_{\ell=1}^4 c_\ell^2 \omega_\ell^2$, the solution of (6) can be obtained via the method of Langrangian multipliers, which yields the here uniquely solvable linear system

$$\begin{pmatrix} \mathbf{D} & \mathbf{Q}^T \\ \mathbf{Q} & \mathbf{0} \end{pmatrix} \begin{pmatrix} \mathbf{c} \\ \mathbf{d} \end{pmatrix} = \begin{pmatrix} \mathbf{0} \\ \mathbf{p} \end{pmatrix}, \quad (7)$$

with diagonal matrix $\mathbf{D} = \mathrm{diag}(\omega_1^2, \omega_2^2, \omega_3^2, \omega_4^2)$ and an auxiliary multiplier vector $\mathbf{d} = (\lambda_1, \lambda_2, \lambda_3)$. Consequently, the interpolated Whitney sources were formed using 8 (the four nodes of the tetrahedron that contains $\vec{r}$ and, for each of the four faces of this tetrahedron the remaining node of the adjacent tetrahedron, i.e., all nodes of overall 5 tetrahedra) nodal basis functions per dipole approximation in a tetrahedral mesh (Table III). This minimal symmetric configuration was used to keep the interpolation as local as possible, which is

Fig. 2. Left: To approximate a dipole with an arbitrary orientation, the position based optimization (PBO) method utilizes a minimal symmetric combination of elements including a given tetrahedron (dark grey) together with those that share a face with it (light grey). Right: In case that a very accurate tetrahedralization in the middle of the grey matter compartment (light grey) has been produced, source locations and radially inwards-pointing source orientations can be fixed [32], [33].

beneficial when sources need to be placed in a narrow grey or white matter layer within a brain geometry (Figure 2, right).

Note that in its current context, our Whitney source model can be generalized to the complete set of piecewise linear tetrahedral $H(\mathrm{div})$ finite elements: It is valid for all Nédélec's edge-based face functions (see formula (15) in the Appendix).

C. Reference Methods

The reference methods give an alternative definition for the right-hand side of equation (1).

1) Partial Integration: In the partial integration (PI) approach [21], [22], a dipole moment $\vec{p}$ placed at $\vec{r}$ is approximated by calculating $\mathbf{f}$ via the formula

$$\begin{aligned} f_i &= -\int_\Omega (\nabla\cdot\vec{J}^p)\psi_i dV = \int_\Omega \vec{J}^p\cdot\nabla\psi_i dV - \int_{\partial\Omega}\partial_{\mathbf{n}}\vec{J}^p\cdot\psi_i dS \\ &= \int_\Omega \vec{J}^p\cdot\nabla\psi_i dV = \begin{cases}\vec{p}\cdot\nabla\psi_i|_{\vec{r}}, & \text{if } \vec{r} \text{ in support of } \psi_i,\\ 0, & \text{otherwise,}\end{cases} \end{aligned} \tag{8}$$

which follows from the limit formulation of the mathematical dipole [21], [31]. The boundary term in the above formula vanishes because the primary currents are limited to the cortical compartment (see Figure 2). One can see that a dipole located inside a given tetrahedral element results in precisely four non-zero vector entries, i.e., the number of nodes on which charges are placed, when the basis functions are linear (Table III).

2) St. Venant Method: The St. Venant approximation [18], [19], [20] of a dipole moment $\vec{p}$ at $\vec{r}$ was obtained by placing monopolar loads $m_0, m_1, m_2, \ldots, m_K$ at the finite element node closest to the source position, $\vec{r}_0$, and at nodes $\vec{r}_1, \vec{r}_2, \ldots, \vec{r}_K$ sharing an edge with $\vec{r}_0$. The net effect of the monopoles was required to be asymptotically a dipole field via

$$\begin{aligned} 0 &= \sum_{i=0}^{K} m_i \\ \frac{1}{\alpha}\vec{p} &= \sum_{i=0}^{K}\frac{m_i}{\alpha}(\vec{r}_i-\vec{r}) \\ 0 &= \sum_{i=0}^{K}\frac{m_i}{\alpha^2}[(\vec{r}_i-\vec{r})\cdot\vec{e}_j]^2 \quad \text{for} \quad j=1,2,3, \end{aligned} \tag{9}$$

where $\vec{e}_j$ for $j = 1,2,3$ are the Cartesian unit vectors and α is a suitably chosen reference distance (here $\alpha = 20$ mm) such that $\alpha > \|\vec{r}_i - \vec{r}_0\|_2$ for all i. From top to bottom, these equations correspond to conservation of charge, approximation of the dipole moment and suppression of higher order moments. For each simulated dipole, the load vector $\mathbf{m} = (m_1, m_2, \ldots, m_K)$ was computed via the standard regularized least-squares procedure given by $\mathbf{m} = (\mathbf{P}^T\mathbf{P} + \lambda\mathbf{D})^{-1}\mathbf{P}^T\mathbf{b}$, where

$$\mathbf{b} = \begin{pmatrix}\mathbf{b}_1\\ \mathbf{b}_2\\ \mathbf{b}_3\end{pmatrix} \quad \text{and} \quad \mathbf{P} = \begin{pmatrix}\mathbf{P}_1\\ \mathbf{P}_2\\ \mathbf{P}_3\end{pmatrix}, \tag{10}$$

with $\mathbf{b}_j = (0, \alpha^{-1}p_j, 0)$ and

$$\mathbf{P}_j = \begin{pmatrix} 1 & \cdots & 1 \\ \alpha^{-1}(\vec{r}_1-\vec{r})\cdot\vec{e}_j & \cdots & \alpha^{-1}(\vec{r}_K-\vec{r})\cdot\vec{e}_j \\ \alpha^{-2}[(\vec{r}_1-\vec{r})\cdot\vec{e}_j]^2 & \cdots & \alpha^{-2}[(\vec{r}_K-\vec{r})\cdot\vec{e}_j]^2 \end{pmatrix}, \tag{11}$$

and $\mathbf{D} = \mathrm{diag}(\|\vec{r}_1-\vec{r}\|^2, \|\vec{r}_2-\vec{r}\|^2, \ldots, \|\vec{r}_K-\vec{r}\|^2)$ is a regularization matrix multiplied by the parameter $\lambda > 0$ (here $\lambda = 10^{-6}$). In a tetrahedral mesh the number of incorporated nodes K is usually around 27 (Table III).

D. Numerical Experiments

Compartment	Scalp	Skull	CSF	Brain
Outer shell radius (mm)	92	86	80	78
Conductivity (S/m)	0.33	0.0042	1.79	0.33

TABLE II
PARAMETRIZATION FOR THE ISOTROPIC FOUR-LAYER SPHERE MODEL.

The numerical experiments of this study concern a four-layer head model composed of concentric spherical origin-centric scalp, skull, cerebrospinal fluid (CSF) and brain tissue compartments with radii and isotropic conductivity values given in Table II. For such multi-compartment sphere models, analytic solutions exist for the potential of a mathematical point dipole [34] to validate our numerical results.

A tetrahedral mesh was generated utilizing a constrained Delaunay tetrahedralization (CDT) approach with maximal tetrahedron volume of 1.12 mm^3 using the software Tetgen [35]. The resulting mesh consists of 801,633 vertices and 4,985,234 elements.

To gather the data, 200 measurement electrodes were distributed regularly over the outer surface of the model. Evaluation of numerical versus analytical solutions will be carried out at those electrode positions.

For the sources, the following eccentricities are studied: 0.2, 0.4, 0.6, 0.8, and 0.99.

E. Evaluation Method

A simulated potential vector $\mathbf{u}_{\text{sim}} \in \mathbb{R}^{200}$ is compared to the corresponding analytic solution $\mathbf{u}_{\text{ana}} \in \mathbb{R}^{200}$ in terms of the following relative difference and magnitude measures that are here given on a percent scale:

$$\mathrm{RDM}(\mathbf{u}_{\text{ana}}, \mathbf{u}_{\text{sim}}) = \frac{100}{2}\left\| \frac{\mathbf{u}_{\text{ana}}}{\|\mathbf{u}_{\text{ana}}\|_2} - \frac{\mathbf{u}_{\text{sim}}}{\|\mathbf{u}_{\text{sim}}\|_2}\right\|_2, \tag{12}$$

$$\mathrm{MAG}(\mathbf{u}_{\text{ana}}, \mathbf{u}_{\text{sim}}) = 100\left(\frac{\|\mathbf{u}_{\text{sim}}\|_2}{\|\mathbf{u}_{\text{ana}}\|_2} - 1\right). \tag{13}$$

The first one of these estimates the difference due to positional and directional inaccuracies between the analytical and numerical dipole approximation (i.e., topography changes), whereas the latter one measures magnitude discrepancy.

Since the quality of the simulation is known to depend on the local mesh geometry as well as on the intra-element position, it is analyzed statistically via a sample of sources as suggested in [26], including results for the different source eccentricities in separate box-plots. This statistical analysis includes maximum and minimum, indicated by upper and lower error bars, and thereby the total range (TR). Furthermore, it includes the interval between upper and lower

quartile, i.e., the interquartile range (IQR), also knows as the spread, which is marked by a box with a white dash showing the median (see, e.g., Figure 3). A sample size of 200 was utilized for each box-plot bar.

F. Implementation Aspects

To compute the EEG electrode voltages efficiently, the transfer matrix approach was applied [30]. Thereby, the large linear equation system resulting from the finite element discretization of equation (1) only had to be solved once for each electrode (not including the reference electrode) instead of being solved once per source. The forward solution is then obtained by setting up the right-hand side vector $\mathbf{f}$ and a matrix-vector multiplication between the transfer matrix and $\mathbf{f}$. This can be carried out very fast for all considered forward approaches, since they all lead to sparse right-hand sides. The

Source orientation	Whitney	St. Venant	PI
free	8	≈ 27	4
fixed	2	≈ 27	4

TABLE III
THE NUMBER OF FINITE ELEMENT MESH NODES NEEDED TO MODEL A SINGLE DIPOLE SOURCE.

number of non-zero entries in $\mathbf{f}$ is shown in Table III. Consequently, the total forward simulation time was very similar for each tested source model. On an Ubuntu 11.04 Linux PC with Intel Core i7-2600 3.40 GHz CPU and 16 GB RAM, the CPU time for computing $\mathbf{T}$ for each electrode (excluding the reference one) was 8.33 seconds and for the St. Venant model and a single dipole it was 0.5 milliseconds for $\mathbf{Tf}$ (including first the computation of $\mathbf{f}$ and then the multiplication to $\mathbf{T}$).

G. Synthetic Source Positions for Whitney Approach

The first experiment concerns the accuracy of the Whitney type source model for tetrahedral elements: Points (A)–(D) (Figure 1) are tested as synthetic dipole positions under the condition that the Whitney and analytical test sources are parallel. The latter is motivated by the fact that sources in the grey matter compartment are radially inwards-oriented (see [32] and the cat experiments by Creutzfeldt *et al.* [33]) as visualized in Figure 2 (right). Here, our aim is to extend the previously existing knowledge of source positioning [24] as well as to support the current interpolation experiments in which the positions of the analytical sources do not coincide with the synthetic ones.

H. Comparison of Source Modeling Approaches

In the second experiment, the Whitney source model is compared to the St. Venant and PI reference methods.

1) Fixed Source Positions and Orientations: In the first phase, the source positions are fine-tuned so that they are optimal for each model: Given a desired position, the St. Venant method is evaluated at the next node [26], PI approach at the next tetrahedron barycenter [26] and the Whitney source model at the closest mesh-based location of type (D). Dipole orientations are again set to be parallel to the Whitney sources [32], [33] (Figure 2, right), since the reference models do not include a mesh-based vector field or special directions.

2) Random Source Positions and Orientations: In the second phase, the dipole positions and directions are random, i.e., not specifically adapted to a certain model. As the interpolation method for the Whitney model, we use the PBO approach (Section II-B1).

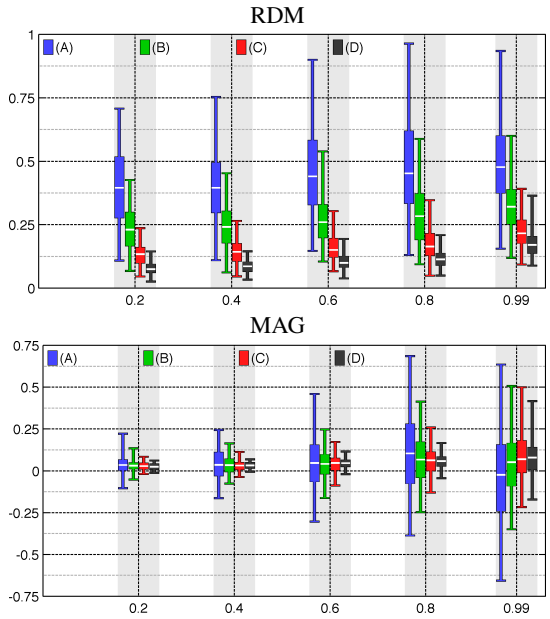

Fig. 3. Synthetic Source Positions for Whitney Approach: RDM (top) and MAG (bottom) for points (A)–(D) as synthetic source positions as shown in Figure 1.

III. Results

A. Synthetic Source Positions for Whitney Approach

Figure 3 presents RDM and MAG for synthetic source positions (A) to (D) as shown in Figure 1. Independently of the source position and over all eccentricities, the RDM and MAG errors are below 1.0% and 0.75%, respectively. Errors and their spread get larger with increasing eccentricity. Overall, the RDM and MAG results suggest that (D) provides the numerically most stable approximation to the given dipole.

With regard to RDM (Figure 3, top) and eccentricity 0.99, position (D) results in an RDM median value of 0.17%. From position (A) to position (D), the IQR is reduced by about 70%.

With regard to MAG (Figure 3, bottom) and eccentricity 0.99, the median values for positions (C) and (D) are nearly identical, while the IQR for (D) is around 30% smaller than for (C).

B. Comparison of Source Modeling Approaches

1) Fixed Source Positions and Orientations: Figure 4 presents the results for the case of fixed source locations and orientations. RDM and MAG errors below 1.5% and 1.0%, respectively, indicate that all three approaches produce numerically accurate results. For all three methods, errors and their spread increase along with the eccentricity. The Whitney model shows the overall best results.

With regard to the RDM (Figure 4, top) and 0.99 eccentricity, the maximal errors for the Whitney model are below 0.4% (St. Venant: $\leq 0.7\%$; PI: $\leq 1.4\%$) and the median value is at 0.2% (St. Venant: 0.3%; PI: 0.7%). The Whitney model yields also the smallest IQR (only 58% and 28% of that of St. Venant and PI, resp.).

With regard to the MAG (Figure 4, bottom) and 0.99 eccentricity, the maximal errors for the Whitney model are below 0.5% (St. Venant: $\leq 0.5\%$; PI: $\leq 0.9\%$) and the median value is nearly optimal for all three methods. The St. Venant approach has the smallest IQR (76% and 39% of that of Whitney and PI, resp.).

2) Random Source Positions and Orientations: In Figure 5, RDM and MAG errors for random source locations and orientations are shown. With RDMs and MAGs below 2.0% and 1.3%, respectively,

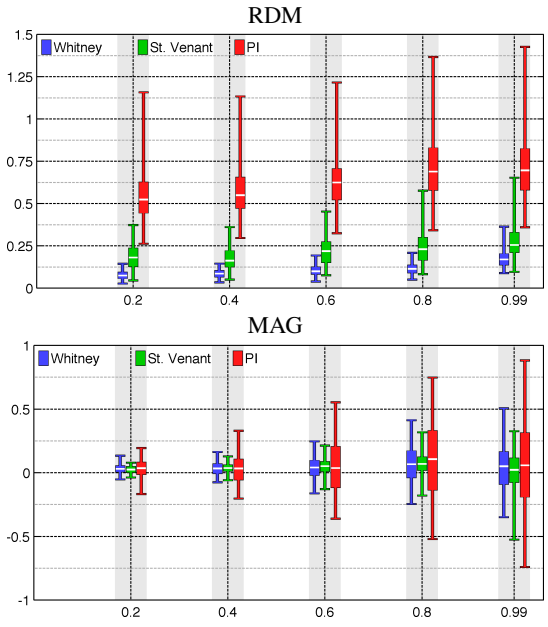

Fig. 4. Fixed Source Positions and Orientations: RDM (top) and MAG (bottom).

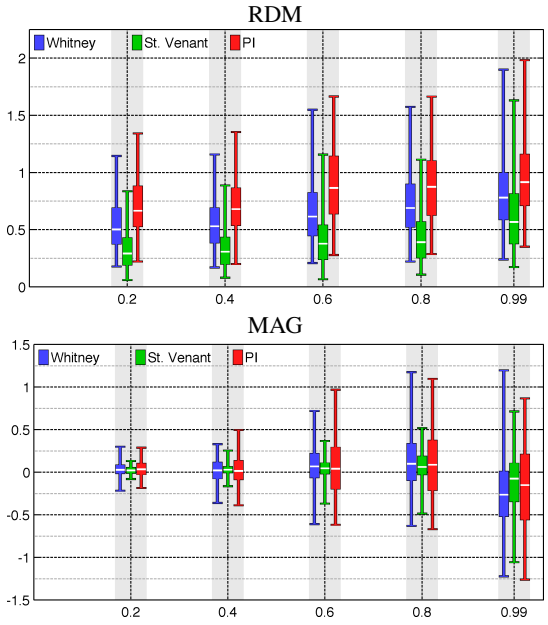

Fig. 5. Random Source Positions and Orientations: RDM (top) and MAG (bottom).

all three approaches produce again low errors. In this comparison, the St. Venant model shows the overall best results. Comparing Figures 4 and 5, one can see that the accuracy of the Whitney model deteriorates significantly in the case of randomized orientations, when multiple basis functions are utilized to represent a single dipole via the PBO interpolation strategy. This is particularly obvious for sources with high eccentricity.

The RDM median (Figure 5, top) increases along with the eccentricity for all three models. At 0.99 eccentricity, the maximal error of the St. Venant model is below 1.6% (Whitney: $\leq$ 1.9%; PI: $\leq$ 2.0%) and the median value is at 0.6% (Whitney: 0.8%; PI: 0.9%). St. Venant and Whitney yield 0.4 % and PI 0.5 % IQR.

With regard to the MAG (Figure 5, bottom) and 0.99 eccentricity, the maximal and median error for St. Venant are 1.1 % (Whitney and PI: 1.3%) and 0.1% (Whitney: 0.3%; PI: 0.2%), respectively. St. Venant also yields the smallest IQR (85% and 59% of that of Whitney and PI, resp.).

IV. Discussion

In this paper, the Whitney (Raviart-Thomas) type source model for finite element method (FEM) based EEG forward modeling was validated utilizing a four-layered spherical head model. A given dipole was approximated as a combination of synthetic positions and dipole moments associated with faces of a single tetrahedron. The results were compared to two widely used direct FEM dipole modeling techniques: the St. Venant [18], [19], [20], [16] and the partial integration (PI) approach [21], [22], [16].

The results in Figure 3 indicate that point (D) out of the tested four positions (A)–(D) performs best as a synthetic source position in terms of both modeling accuracy and reliability. This suggests that a Whitney basis function can be associated with a dipole placed at the midpoint (D) of the two nodes $\vec{r}_1$ and $\vec{r}_4$ (see Figure 1 and equation (5)) that also determine the synthetic dipole moment (see equation (4)). Hence, a Whitney source corresponds to two monopolar loads with opposite sign at locations $\vec{r}_1$ and $\vec{r}_4$, i.e., the simplest possible combination to approximate a dipole with monopolar loads. Moreover, all points (A)–(D) yielded an appropriate modeling accuracy which is important knowledge if the superposition of the Whitney basis functions is treated as a vector field rather than a set of dipoles, that is, if the location of a source is estimated, instead of (D), based on where the actual vector field is strong (see Section II-B1).

Further experiments (see Figure 4) showed that, in approximation of a dipole with fixed location and orientation given by (5) and (4), the Whitney model was overall superior compared to the references. Besides numerical accuracy, another important aspect is the focality of the source model. Also here, the Whitney is the superior one (2 nodes, see Table III), followed by PI (4 nodes) and St. Venant ($\approx$ 27 nodes). From our experience, numerical accuracy is spoiled if monopoles are positioned closer than one element layer from the next conductivity discontinuity. Therefore, if an optimal segmentation and tetrahedralization of the grey matter compartment following the normal constraint can be produced, i.e., sources are only allowed to point radially into the cortex [32], [33] (see Figure 2, right), then the Whitney model seems the currently preferable one.

To produce a cortical segmentation and tetrahedralization as shown in Figure 2 (right) is currently still a challenging task and the normal-constraint can thus not always be recommended. Therefore, further experiments with random locations and orientations were performed (see Figure 5). In this case, the numerical accuracy of the St. Venant approach was slightly superior. However, maximal RDM and MAG errors for all three approaches were smaller than 2%, indicating that other aspects, e.g., with regard to practical applicability such as the focality, should be prioritized. In this aspect, the PI is the best (4 nodes, see Table III), followed by Whitney (8 nodes) and St. Venant ($\approx$ 27 nodes).

For approximation of arbitrary dipoles in a tetrahedral mesh, we used the quadratic element-wise position based optimization (PBO) interpolation of the synthetic dipole moments [31]. The PBO method is an improvement to the pseudoinverse interpolation [25], which guarantees a stable approximation of the dipole moment with a minimal symmetric configuration of four basis functions to allow sources to be positioned in narrow grey or white matter layers. The more accurate PBO strategy takes, in addition to the source orientations, also the positions into account [31], as it tries to find

a matching dipole as close as possible to the given position. Since the PBO algorithm is rather heuristic than implied by the theory of interpolation, it can be a suboptimal one and accuracies above the currently already high level in the percent range might be strived for.

We could, e.g., think of using higher order St. Venant conditions within the Whitney model. Producing a significant improvement to PBO is, however, likely to be difficult, since due to the lack of degrees of freedom, St. Venant type conditions cannot be filled, other than the one for the dipole moment. Consequently, it seems that the current vector sources can be improved by including a larger set of basis functions in approximation of a single dipole, so that additional conditions can be satisfied. Furthermore, the question arises: What would be an optimal number of basis functions in approximation of a single dipole for a realistic head model in which conductivity discontinuities affect the source modeling accuracy? Finding an answer necessitates improvement of the current analysis technique relying on analytic solution that exists for a spherical layered head model. An obvious solution would be to produce an extremely high-resolution reference FEM solution corresponding to a realistic head model, which one can use for evaluation of different interpolation techniques. In addition to these aspects, also the order of interpolation, e.g., quadratic vs. cubic, is a central factor affecting the quality of the results.

Better results can be obtained also by extending the polynomial basis utilized in dipole approximation. This could mean, for instance, complementing the current Whitney type sources with higher-order Nédélec elements [29], [28], which would require also increasing the polynomial order of the potential field [36] to avoid mapping of the added degrees of freedom to zero right-hand side vector entries. In such a context, the cost of the assembly procedure will be significantly larger, such as in the case of the subtraction approach [37], [16], [15]. The source modeling methods of this paper can, in contrast, be considered computationally fast as the right-hand side vectors of the forward problem are sparse due to the linearity of the applied finite element basis. Moreover, implementation of higher-order elements would require not only technical but also theoretical work, since it is not immediately obvious, for example, whether and how the additional degrees of freedom can be associated with dipoles or multipoles: the current case of linear basis functions is special in the sense that it allows a direct (synthetic) dipole interpretation. The same reasoning further motivates development of techniques for handling a vector field independently of the mathematical interpretation of the vector basis, that is here a set of dipoles. An obvious argument supporting such a future direction is also that real neural sources have a finite support. Hence, more crucial than approximation of a single point-wise source can be that of a complete field under *a priori* knowledge on the neural fiber structure such as the previously discussed normal constraint.

The Whitney (Raviart-Thomas) model can potentially be used in any application context where a highly focal source placement is needed, e.g., in a narrow part of the grey matter regarding both non-interpolated and interpolated modalities. Of these, the preferable one depends on several factors, such as the applied inverse methodology. Non-interpolated Whitney type sources have been applied to EEG inversion previously in [38]. The use of a tetrahedral mesh is not necessary for the validity of the Whitney approach. The final section of the appendix shows how Whitney sources can be defined also for a hexahedral mesh. Based on our preliminary experiments in a regular hexahedral grid, the differences to the reference approaches are, however, minor to the tetrahedral case.

Summarizing the above ideas, directions of the future work can include further development of the divergence conforming basis functions in the context of EEG source modeling, e.g., regarding higher polynomial or interpolation orders. Important topics related to the interpolation quality include also investigation of the effect of the conductivity jumps within the brain as well as St. Venant type conditions applied to vector basis functions. Additionally, developing methodology for handling finitely-supported divergence conforming source currents as vector fields, e.g., for advanced inversion purposes [38], [39], is an attractive future objective.

APPENDIX

Linear Nédélec's edge-based face functions span the piecewise linear subspace of $H(\mathrm{div}) = \{\vec{w} \,|\, \nabla \cdot \vec{w} \in L^2(\Omega)\}$ for a tetrahedral mesh [29], [28]. Given face F and edge $E \subset F$, a single basis function restricted to a tetrahedron T (Figure 6) is of the form

$$\vec{w}_{\{E,F,T\}} = c_{\{E,F\}}\, \psi_{\{E,F,T\}}\, \frac{\vec{\ell}_{\{E,T\}}}{V_T} \tag{14}$$

where V_T is the volume of T, the vector $\vec{\ell}_{E,T}$ is the edge opposite to E, oriented according to the right hand rule with respect to E, and $\psi_{\{E,F,T\}}$ is the basis function for the node on F not belonging to E, restricted to a single tetrahedron. Denoting the three edges of face F by E_1, E_2 and E_3 a Whitney (Raviart-Thomas) basis function associated with F can be expressed in T as the mean

$$\vec{w}_{\{F,T\}} = \frac{1}{3}(\vec{w}_{\{E_1,F,T\}} + \vec{w}_{\{E_2,F,T\}} + \vec{w}_{\{E_3,F,T\}}). \tag{15}$$

Hence, Whitney basis functions form a subspace inside the space of linear edge-based face functions: the former has one degree of freedom per face whereas the latter has three. In the current context, both function bases, however, result in the same dipole model, which is shown below.

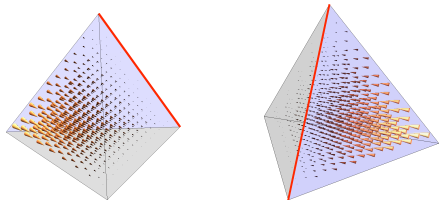

Fig. 6. Two views of a linear Nédélec's edge-based face function restricted to a single tetrahedron T. The face F and edge $E \subset F$ determining the function have been visualized with light blue and red (bold line) color, respectively.

Each linear edge-based face function is supported on two tetrahedra T_1 and T_2 sharing the face F as shown in Figure 1. Defining

$$c_{\{E,F\}} := \frac{4}{\|\vec{\ell}_{\{E,T_1\}} + \vec{\ell}_{\{E,T_2\}}\|} \tag{16}$$

the synthetic dipole moment is a unit vector given by

$$\begin{aligned}
\vec{q}_{\vec{w}} &= \int_\Omega \vec{w}_{\{E,F\}}\, dV \\
&= c_{\{E,F\}}\, \frac{\vec{\ell}_{\{E,T_1\}}}{V_{T_1}} \int_{T_1} \psi_{\{E,F,T_1\}}\, dV \\
&\quad + c_{\{E,F\}}\, \frac{\vec{\ell}_{\{E,T_2\}}}{V_{T_2}} \int_{T_2} \psi_{\{E,F,T_2\}}\, dV \\
&= c_{\{E,F\}}\, \frac{\vec{\ell}_{\{E,T_1\}}}{V_{T_1}}\, \frac{V_{T_1}}{4} + c_{\{E,F\}}\, \frac{\vec{\ell}_{\{E,T_2\}}}{V_{T_2}}\, \frac{V_{T_2}}{4} \\
&= \frac{\vec{\ell}_{\{E,T_1\}} + \vec{\ell}_{\{E,T_2\}}}{\|\vec{\ell}_{\{E,T_1\}} + \vec{\ell}_{\{E,T_2\}}\|}.
\end{aligned} \tag{17}$$

Here, the fact that $\int_T \psi\, dV = V_T/4$, i.e., any linear nodal basis function ψ integrated over T equals $V_T/4$, has been used. Assuming

that the vector flux is inbound in T_1 and outbound in T_2, it holds that $\nabla\psi_{\{E,F,T_1\}}\cdot\vec{\ell}_{\{E,T_1\}} = -\nabla\psi_{\{E,F,T_2\}}\cdot\vec{\ell}_{\{E,T_2\}} = 1$, since the linear function $\psi_{\{E,F,T\}}$ grows from zero to one on a path corresponding to (positive or negative) vector $\vec{\ell}_{\{E,T_1\}}$. Consequently, it follows that the entry of matrix $\mathbf{G}$ corresponding to (global) basis functions ψ and $\vec{w}$ is of the form

$$\begin{aligned} G_{\psi,\vec{w}} &= -\int_\Omega (\nabla\cdot\vec{w})\ \psi\ dV \\ &= -c_{\{E,F\}}\ \nabla\psi_{\{E,F,T_1\}}\cdot\frac{\vec{\ell}_{\{E,T_1\}}}{V_{T_1}}\ \int_{T_1}\ \psi\ dV \\ &\quad -c_{\{E,F\}}\ \nabla\psi_{\{E,F,T_2\}}\cdot\frac{\vec{\ell}_{\{E,T_2\}}}{V_{T_2}}\ \int_{T_2}\ \psi\ dV \\ &= \frac{s_{\{\psi,T_1\}}-s_{\{\psi,T_2\}}}{\|\vec{\ell}_{\{E,T_1\}}+\vec{\ell}_{\{E,T_2\}}\|} \end{aligned} \tag{18}$$

in which $s_{\{\psi,T\}} = 1$, if ψ is supported on T, and otherwise $s_{\{\psi,T\}} = 0$. Using the node indices of Figure 1, one can write

$$\begin{aligned} \vec{q}_{\vec{w}} &= \frac{\vec{r}_4-\vec{r}_1}{\|\vec{r}_4-\vec{r}_1\|} \\ G_{\psi,\vec{w}} &= \frac{s_{\{\psi,T_1\}}-s_{\{\psi,T_2\}}}{\|\vec{r}_4-\vec{r}_1\|}. \end{aligned} \tag{19}$$

Consequently, the Whitney source model of this paper is, in fact, a general one in the current context of divergence conforming $H(\mathrm{div})$ vector fields, piecewise linear basis functions and a tetrahedral mesh. Notice also that Equation (3) follows from the formulae above, and that the formulation for $\vec{q}_{\vec{w}}$ given in [25] simplifies to the current one due to similarity under scaling.

1) Whitney Elements for a Hexahedral Mesh: A Whitney basis function of a hexahedral mesh is supported on two adjacent hexahedra Q_1 and Q_2 (Figure 7) sharing a face and aligned with coordinate axes. For x-direction, it can be defined as follows:

$$\vec{w}_k(x,y,z) = \begin{cases} \dfrac{2}{(a_1-a_2)bc}\left(1-\dfrac{x}{a_1}\right)\vec{e}_1, & \text{if} \quad (x,y,z)\in Q_1 \\ \dfrac{2}{(a_1-a_2)bc}\left(1+\dfrac{x}{a_2}\right)\vec{e}_1, & \text{if} \quad (x,y,z)\in Q_2 \\ 0, & \text{otherwise,} \end{cases} \tag{20}$$

where constants $a_1 > 0, a_2 < 0, b > 0$ and $c > 0$ are as in Figure 7. The basis function is a piecewise first order polynomial with the normal component continuous on the shared face and zero on all other faces. As dipole position $\mathbf{x}_0$, we chose the midpoint of S with coordinates $(0, \frac{b}{2}, \frac{c}{2})$ in the reference element (Figure 7). Note that the synthetic dipole moment for (20) is given by $\vec{q} = \int_\Omega \vec{w}\ dV = \vec{e}_1$. The other coordinate directions follow analogously. In a hexahedral mesh, 20 Whitney basis functions are needed to approximate a dipole.

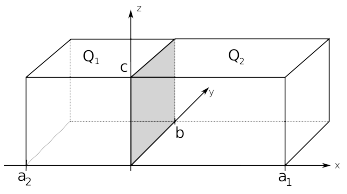

Fig. 7. Two reference hexahedrons

ACKNOWLEGMENT

SP was supported by the Academy of Finland (project 257288). JV and CW were supported by the Priority Program 1665 of the Deutsche Forschungsgemeinschaft (DFG) (project WO1425/5-1) and by EU project ChildBrain (Marie Curie Innovative Training Networks, grant agreement no. 641652).

REFERENCES

[1] E. Niedermeyer and F. L. da Silva, *Electroencephalography: Basic Principles, Clinical Applications, and Related Fields, Fifth Edition*. Philadelphia: Lippincott Williams & Wilkins, 2004.

[2] M. A. B. Brazier and University of California, Los Angeles. Brain Research Institute, *Computer techniques in EEG analysis*, ser. Electroencephalography and clinical neurophysiology: Supplement. Amsterdam: Elsevier Pub. Co., 1961.

[3] D. Braess, *Finite Elements*. Cambridge: Cambridge University Press, 2001.

[4] C. Wolters, R. Beckmann, A. Rienäcker, and H. Buchner, "Comparing regularized and non-regularized nonlinear dipole fit methods: A study in a simulated sulcus structure," *Brain Topography*, vol. 12, no. 1, pp. 3–18, 1999, http://dx.doi.org/10.1023/A:1022281005608, PMID: 10582561.

[5] J. de Munck, C. Wolters, and M. Clerc, "EEG & MEG forward modeling." in *Handbook of Neural Activity Measurement*, R. Brette and A. Destexhe, Eds. Cambridge University Press, New York, 2012.

[6] J. Kybic, M. Clerc, T. Abboud, O. Faugeras, R. Keriven, and T. Papadopoulo, "A common formalism for the integral formulations of the forward EEG problem," *IEEE Trans. Med. Imag.*, vol. 24, no. 1, pp. 12–18, 2005.

[7] Y. Ataseven, Z. Akalin-Acar, C. E. Acar, and N. G. Gencer, "Parallel implementation of the accelerated BEM approach for EMSI of the human brain," *Med. Biol. Eng. Comput.*, vol. 46, no. 7, pp. 671–679, 2008.

[8] M. Stenroos and J. Sarvas, "Bioelectromagnetic forward problem: isolated source approach revis(it)ed." *Phys.Med.Biol.*, vol. 57, no. 11, pp. 3517–3535, 2012.

[9] J. Ermer, J. C. Mosher, S. Baillet, and R. M. Leahy, "Rapidly recomputable EEG forward models for realistic head shapes," *Physics in Medicine and Biology*, vol. 46, pp. 1265–1281, 2001.

[10] K. Wendel, N. Narra, M. Hannula, P. Kauppinen, and J. Malmivuo, "The influence of CSF on EEG sensitivity distributions of multilayered head models." *IEEE Trans. Biomed. Eng.*, vol. 55, no. 4, pp. 1454–1456, 2008.

[11] J. Vorwerk, J.-H. Cho, S. Rampp, H. Hamer, T. Knösche, and C. Wolters, "A guideline for head volume conductor modeling in EEG and MEG." *NeuroImage*, vol. 100, pp. 590–607, 2014.

[12] M. Dannhauer, B. Lanfer, C. Wolters, and T. Knösche, "Modeling of the human skull in EEG source analysis," *Human Brain Mapping*, vol. 32, no. 9, pp. 1383–1399, 2011, dOI: 10.1002/hbm.21114, PMID: 20690140.

[13] H. Hallez, B. Vanrumste, P. Van Hese, S. Delputte, and I. Lemahieu, "Dipole estimation errors due to differences in modeling anisotropic conductivities in realistic head models for EEG source analysis." *Phys.Med.Biol.*, vol. 53, pp. 1877–1894, 2008.

[14] D. Güllmar, J. Haueisen, and J. Reichenbach, "Influence of anisotropic electrical conductivity in white matter tissue on the EEG/MEG forward and inverse solution. a high-resolution whole head simulation study." *NeuroImage*, 2010, doi:10.1016/j.neuroimage.2010.02.014.

[15] C. Wolters, H. Köstler, C. Möller, J. Härtlein, L. Grasedyck, and W. Hackbusch, "Numerical mathematics of the subtraction method for the modeling of a current dipole in EEG source reconstruction using finite element head models." *SIAM J. on Scientific Computing*, vol. 30, no. 1, pp. 24–45, 2007, http://dx.doi.org/10.1137/060659053.

[16] S. Lew, C. H. Wolters, T. Dierkes, C. Röer, and R. S. MacLeod, "Accuracy and run-time comparison for differential potential approaches and iterative solvers in finite element method based EEG source analysis," *Applied Numerical Mathematics*, vol. 59, pp. 1970–1988, 2009.

[17] T. Medani, D. Lautru, and Z. Ren, "Study of Modeling of Current Dipoles in the Finite Element Method for EEG Forward Problem," in *Conference NUMELEC 2012*, Marseille, France, Jul. 2012, p. On line. [Online]. Available: http://hal.upmc.fr/hal-00754433

[18] R. Schönen, A. Rienäcker, R. Beckmann, and G. Knoll, "Dipolabbildung im FEM-Netz, Teil I," RWTH Aachen, Arbeitspapier zum Projekt Anatomische Abbildung elektrischer Aktivität des Zentralnervensystems, Juli 1994.

[19] H. Buchner, G. Knoll, M. Fuchs, A. Rienäcker, R. Beckmann, M. Wagner, J. Silny, and J. Pesch, "Inverse localization of electric dipole current sources in finite element models of the human head," *Electroencephalogr Clin Neurophysiol.*, vol. 102, 1997.

[20] R. Toupin, "Saint-Venant's principle," *Archive for Rational Mechanics and Analysis*, vol. 18, no. 2, pp. 83–96, 1965. [Online]. Available: http://dx.doi.org/10.1007/BF00282253

[21] Y. Yan, P. L. Nunez, and R. T. Hart, "Finite-element model of the human head: scalp potentials due to dipole sources," *Med Biol Eng Comput.*, vol. 29, no. 5, pp. 475–81, 1991.

[22] D. Weinstein, L. Zhukov, and C. Johnson, "Lead-field bases for electroencephalography source imaging," *Ann Biomed Eng.*, vol. 28, no. 9, pp. 1059–65, 2000.

[23] O. Tanzer, S. Järvenpää, J. Nenonen, and E. Somersalo, "Representation of bioelectric current sources using whitney elements in the finite element method," *Physics in Medicine and Biology*, vol. 50, pp. 3023–3039, 2005.

[24] S. Pursiainen, A. Sorrentino, C. Campi, and M. Piana, "Forward simulation and inverse dipole localization with lowest order Raviart-Thomas elements for electroencephalography," *Inverse Problems*, vol. 27, no. 4, p. 045003 (18pp), 2011.

[25] S. Pursiainen, "Raviart-Thomas -type sources adapted to applied eeg and meg: implementation and results," *Inverse Problems*, vol. 28, no. 6, p. 065013, 2012.

[26] J. Vorwerk, "Comparison of Numerical Approaches to the EEG Forward Problem," Master's thesis, Universität Münster, 2011.

[27] L. Evans, *Partial Differential Equations*, ser. Graduate studies in mathematics. American Mathematical Society, 1998.

[28] M. Ainsworth and J. Coyle, "Hierarchic finite elements for unstructured tetrahedral meshes," *Int. J. Numer. Meth. Engng*, vol. 58, pp. 2103–2130, 2003.

[29] P. Monk, *Finite Element Methods for Maxwell's Equations*. Oxford, UK: Clarendon Press, 2003.

[30] C. Wolters, L. Grasedyck, and W. Hackbusch, "Efficient computation of lead field bases and influence matrix for the FEM-based EEG and MEG inverse problem," *Inverse Problems*, vol. 20, no. 4, pp. 1099–1116, 2004, http://dx.doi.org/10.1088/0266-5611/20/4/007.

[31] M. Bauer, "Special Finite Elements for Dipole Modelling," Master's thesis, University Erlangen-Nuremberg, 2012.

[32] R. Schmidt and G. Thews, *Physiologie des Menschen*. 24. Auflage, Springer-Verlag Berlin Heidelberg, 1990.

[33] O. Creutzfeldt, G. Fromm, and H. Kapp, "Influence of transcranial d-c currents on cortical neuronal activity." *Experimental Neurology*, vol. 5, pp. 436–452, 1962.

[34] J. de Munck and M. Peters, "A fast method to compute the potential in the multi sphere model," *IEEE Trans Biomed. Eng.*, vol. 40, no. 11, pp. 1166–1174, 1993.

[35] H. Si, "TetGen: A quality tetrahedral mesh generator and three-dimensional delaunay triangulator," *Weierstrass Institute for Applied Analysis and Stochastic, Berlin, Germany*, 2006, `http://tetgen.berlios.de`.

[36] S. Pursiainen, "EEG/MEG forward simulation through h- and p-type finite elements," *Journal of Physics: Conference Series*, vol. 124, no. 1, p. 012041, 2008. [Online]. Available: http://stacks.iop.org/1742-6596/124/i=1/a=012041

[37] F. Drechsler, C. Wolters, T. Dierkes, H. Si, and L. Grasedyck, "A full subtraction approach for finite element method based source analysis using constrained delaunay tetrahedralisation." *NeuroImage*, vol. 46, no. 4, pp. 1055–1065, 2009, http://dx.doi.org/10.1016/j.neuroimage.2009.02.024, PMID: 19264145.

[38] D. Calvetti, H. Hakula, S. Pursiainen, and E. Somersalo, "Conditionally Gaussian hypermodels for cerebral source localization," *SIAM J. Imaging Sci.*, vol. 2, no. 3, pp. 879–909, 2009.

[39] F. Lucka, S. Pursiainen, M. Burger, and C. H. Wolters, "Hierarchical bayesian inference for the EEG inverse problem using realistic FE head models: Depth localization and source separation for focal primary currents," *NeuroImage*, vol. 61, no. 4, pp. 1364–1382, 2012.

Martin Bauer Martin Bauer received his MSc in Computational Engineering in 2012 at the Friedrich-Alexander University (FAU) in Erlangen, Germany. He is working as a research assistant at the Chair for System Simulation. Main research interests are high performance computing and development of massively parallel algorithms and software packages, especially in the context of fluid dynamics simulations using the lattice Bolzmann method.

Sampsa Pursiainen received his MSc(Eng) and PhD(Eng) degrees (Mathematics) in the Helsinki Univ. of Tech. (Aalto Univ. since 2010), Espoo, Finland, in 2003 and 2009. He focuses on forward and inversion techniques of applied mathematics. In 2010–11 he stayed at the Dept. of Math., Univ. of Genova, Italy collaborating also with the Inst. for Biomagnetism and Biosignalanalysis (IBB), Univ. of Münster, Germany. He has been a postdoctoral researcher of the Academy of Finland (257288) in 2012–15. In 2015, he continues his work as an Assistant Prof. at the Dept. of Math., Tampere Univ. of Tech., Finland.

Johannes Vorwerk received the M.Sc. degree in mathematics with a minor in physics from the University of Münster, Münster, Germany, in 2011. Since then, he is working towards the Ph.D. degree at the Institute for Biomagnetism and Biosignalanalysis (IBB) at the University of Münster, Münster, Germany.
His research interests include EEG/MEG source localization with a focus on solving the EEG/MEG forward problem using FE methods and tCS optimization.

Harald Köstler Harald Köstler finished his Ph.D. in 2008 on parallel multigrid methods in medical image processing. Currently, he is a researcher at the Chair for System Simulation in Erlangen, Germany. His research interests include software engineering concepts for simulation software on HPC clusters, multigrid methods, and programming techniques for parallel hardware, especially GPUs.

Carsten H. Wolters received the M.Sc. degree in Mathematics with a minor in Medicine from the RWTH Aachen, Aachen, Germany, the Ph.D. degree in Mathematics from the University of Leipzig, Leipzig, Germany and the Habilitation in Mathematics from the University of Münster, Münster, Germany, in 1997, 2003 and 2008, respectively. From 1997 to 2004, he was with the Max Planck Institutes for Human Cognitive and Brain Sciences and Mathematics in the Sciences, Leipzig, Germany. In 2004, he joined the Scientific Computing and Imaging Institute at the University of Utah, Salt Lake City, USA. Since 2005, he is a Research Associate with the Institute for Biomagnetism and Biosignalanalysis (IBB) at the University of Münster, Münster, Germany. Since 2008, he is heading the research group "Methods in Bioelectromagnetism" at IBB. His research interests are in the field of neuroscience with a focus on reconstructing and manipulating neuronal networks in the human brain.